Thermoacoustic Heat Engine Modeling and Design Optimization*

Andrew C. Trapp[†] Florian Zink[‡] Oleg A. Prokopyev[§]
Laura Schaefer[¶]

July 27, 2011

Abstract

Thermoacoustic heat engines (TAEs) are potentially advantageous drivers for thermoacoustic refrigerators (TARs). Connecting TAEs to TARs means that waste heat can effectively be utilized to provide cooling, and increase overall efficiency. However, this is currently a niche technology. Improvements can be made through a better understanding of the interactions of relevant design parameters. This work develops a novel mathematical programming model to optimize the performance of a simple TAE. The model consists of system parameters and constraints that capture the underlying thermoacoustic dynamics. We measure the performance of the engine with respect to several acoustic and thermal objectives (including work output, viscous losses and heat losses). Analytical solutions are presented for cases of single objective optimization that identify globally optimal parameter levels. We also consider optimizing multiple objective components simultaneously and generate the efficient frontier of Pareto optimal solutions corresponding to selected weights.

Keywords: Thermoacoustics; Mathematical Programming; Global Optimization; Multiobjective Optimization; Efficient Frontier

1 Introduction

The goal of this work is to demonstrate how optimization techniques can improve the design of thermoacoustic devices. Thermoacoustic devices utilize sound waves instead of mechanical pistons to drive a thermodynamic process. One of their advantages is the inherent mechanical simplicity. While this concept is not new, the technology has not been advanced to a high degree, as compared to, for example, the internal combustion engine. After reviewing some

*Corresponding author: O.A. Prokopyev. E-mail: prokopyev@engr.pitt.edu
[†]Worcester Polytechnic Institute, School of Business, Worcester, MA 01609
[‡]IAV GmbH, Rockwellstr. 16, 38518 Gifhorn, Germany
[§]Department of Industrial Engineering, University of Pittsburgh, Pittsburgh, PA 15261
[¶]University of Pittsburgh, Department of Mechanical Engineering and Material Science, 153 Benedum Hall, Pittsburgh, PA 15261

fundamental physical properties underlying thermoacoustic devices, we will then proceed to discuss our approach to optimize their design.

The Stirling cycle, developed in 1816 Garrett [1999], is the basic thermodynamic cycle occurring in thermoacoustic devices. The original mechanical Stirling engine utilized two pistons and a regenerative heat exchanger Kaushik and Kumar [2000]. Over the course of one cycle, the working gas is compressed; it then transfers thermal energy to the heat sink, thus maintaining a constant temperature. Afterwards, the gas is heated at constant volume by the regenerator and then is heated further at the heat source. This heat supply occurs while the gas is allowed to expand and drive the power piston, again at constant temperature. After expansion, the gas is displaced to the heat sink, while cooling off at constant volume by depositing heat to the regenerator, which stores heat between cycle segments Kaushik and Kumar [2000]. It is noteworthy that this externally heated, closed cycle uses the same gas for all stages, as opposed to the internal combustion engine, which has a constant throughput of working gas and fuel. The first application of this cycle as a thermoacoustic technology occurred when Ceperley recognized that sound waves could replace pistons for gas compression and displacement Ceperley [1985]. Since then, a wide variety of thermoacoustic engines (TAEs) and their counterpart, thermoacoustic refrigerators (TARs), have been developed. TAEs utilize a heat input to create intense sound output, while TARs can utilize this intense sound to withdraw energy from their surroundings.

1.1 Thermoacoustic Engines

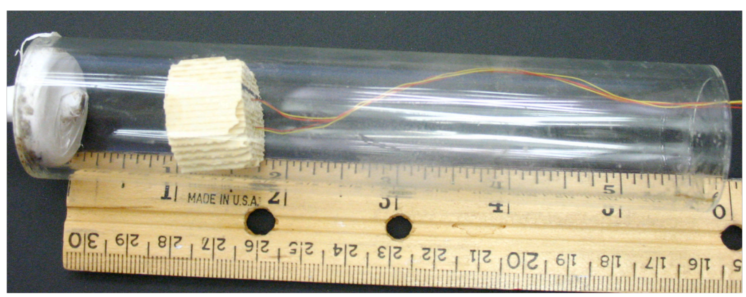

Figure 1: A simple standing wave engine demonstrator

The key component in thermoacoustic devices is a porous regenerative unit known as a stack. This unit is sandwiched between two heat exchangers, one to supply heat at high temperature on the order of several hundred degrees Celsius, the other to withdraw heat from the system at (ideally) ambient temperature. In practice, the cold side must be cooled because of conduction of heat from the hot side to the cold side, thus heating the cold side to temperatures higher than ambient. The temperature gradient across the regenerative unit results in amplification of pressure disturbances in the working gas and a corresponding loud noise to be emitted once a steady state has been achieved. In order for amplification to occur, this temperature gradient must be larger than the critical temperature gradient, which is related to the temperature gradient that the gas would experience if it were under the influence of a sound wave in adiabatic conditions. The expression for this critical temperature gradient was derived by Swift Swift [2002] and is given in equation (1):

$$\nabla T_{crit} = \frac{\omega p}{\rho_m c_p u}. \tag{1}$$

This critical temperature gradient depends on the operating frequency ω, the first order pressure p and velocity u in the standing wave, as well as the mean gas density ρ_m and specific heat c_p. In a TAE, the imposed temperature gradient must be greater than this critical temperature gradient $\frac{dT/dx}{dT/dx_{crit}} > 1$, while in TARs the critical temperature gradient upper bounds its performance $\frac{dT/dx}{dT/dx_{crit}} < 1$ Xiao [1995]. Figure 1 shows a very simple prototypical standing wave, quarter-wavelength TAE.

The closed end of the resonance tube is the pressure antinode and the velocity node; by locating the porous stack near the closed end, the interior gas experiences large pressure oscillations and relatively small displacement. A heating wire provides the heat input, causing a temperature gradient to be established across the stack (in the axial direction). When a gas in the vicinity of the walls inside the regenerative unit is subject to a sound wave, it experiences compression, expansion, and displacement. Over the course of the cycle, heat is added to the gas at high pressure, and heat is withdrawn from it at low pressure. This energy imbalance results in an increase of the pressure amplitude from one cycle to the next, until the acoustic dissipation of the sound energy equals the addition of heat to the system Swift et al. [2000], Bastyr and Keolian [2003], Poese et al. [2004], Backhaus and Swift [2000].

In order to better visualize this phenomenon, we draw a parallel to optics. The amplification of the acoustic wave is similar to an optical laser, where light waves travel between a mirror and a partially silvered mirror in a standing wave fashion. Through resonance, the light waves are amplified and eventually released through the partially mirrored side as a high power laser beam. The amplified sound waves in a thermoacoustic engine can likewise be extracted from the resonance tube to power external devices Garrett [2000]. Thermoacoustic engines are predominantly used to drive TARs, which utilize the reverse Stirling cycle to attenuate the pressure in a sound wave and thereby withdrawing heat from the surroundings. Several examples of such devices are given in the literature Poese et al. [2004], Kagawa [2000], Tang et al. [2007], Vanapalli et al. [2007]. Both the engine and the refrigerator share the regenerative unit as their key component. This regenerative unit is responsible for both the creation of sound/cooling, as well as viscous losses and heat flows that are counterproductive to thermoacoustic energy conversion.

1.2 Optimization in Thermoacoustics

Thermoacoustic technology is not nearly as advanced as the internal combustion engine, which has experienced significant advances since its conception over a century ago. One of the main reasons for its limited use is the poor cycle performance in comparison to the internal combustion engine Herman and Travnicek [2006]. In particular, it is the tradeoffs between the acoustic and thermal parameters that are not well understood. These complex interactions can be better understood through mathematical analysis and optimization, a design aid that is under-utilized in the thermoacoustic community. Some existing efforts include Zink et al. Zink et al. [2009], who use an optimization-based approach in conjunction with a finite element solver to identify (locally) optimal solutions to their two-variable model. Another study is Minner et al. Minner et al. [1997], who consider the optimization of a thermoacoustic refrigeration system. They use extensive model development and seek to optimize the coefficient of performance, considering geometric parameters and fluid properties of the system and the Nelder-Mead simplex algorithm to search for a (locally) optimal solution. However, in order to account for the thermoacoustic operating conditions, they use

DeltaE extensively. DeltaE is a blackbox simulation tool based on linear acoustic theory developed by Swift et al. Swift [2002] that considers a thermoacoustic device as a combination of individual sections. It analyzes each section in regard to its acoustic properties and the velocity, pressure, and temperature behavior.

Both Wetzel Wetzel [1998] and Besnoin Besnoin [2001] discuss thermoacoustic device optimization in their works. While Wetzel focuses on the optimal performance of a thermoacoustic refrigerator, Besnoin targets heat exchangers. In addition to these optimization efforts, Zoontjens Zoontjens et al. [2006] illustrates the optimization of inertance sections of thermoacoustic devices; they also use DeltaE to vary individual parameters to determine optimal designs. Ueda Ueda et al. [2003] determines the effect of a variation of certain engine parameters on pressure amplitudes. Another work that makes use of DeltaE is Tijani et al. Tijani et al. [2002], who attempt to optimize the spacing of the stack.

1.3 Goals of the present work

While the previous works are valuable additions to the field of thermoacoustics, most studies (the exception being the Zink et al. Zink et al. [2009] and Minner et al. Minner et al. [1997] studies) vary only a single parameter, holding all else fixed. Such parametric studies are unable to capture the nonlinear interactions inherent in thermoacoustic models with multiple variables, and can only guarantee locally optimal solutions. In contrast, our model allows for the simultaneous varying of multiple parameters to identify globally optimal values. Additionally, our model considers several contrasting acoustic and thermal objectives, where unlike previous studies we incorporate heat losses to the surroundings occurring with normal device operation. Because optimizing with respect to such losses may be less intuitive than the more obvious goals of maximizing power output or efficiency, we provide a magnitude estimate in Section 2.1.2 to justify their inclusion. The presence of these contrasting objectives permits the additional modeling flexibility of using weights to place desired objective component emphasis in the context of multiobjective optimization (see also discussion in Section 2.1). Optimal solutions corresponding to specific objective weights can be used to construct the efficient frontier of Pareto optimal solutions.

The remainder of this paper is organized in the following fashion: the fundamental components of our mathematical model characterizing the standing wave thermoacoustic Sterling heat engine are presented in Section 2. In Section 3, we discuss single objective optimization, using analytical approaches to find values of the variables that satisfy the constraints and are globally optimal with respect to the considered objective function. Section 4 considers multiobjective optimization. In Section 5, we conclude by suggesting possible future extensions of this work, and in Section 7 we provide a concise summary of the key terminology used in this paper.

2 TAE Modeling

In this section we describe the mathematical model we use to represent the underlying dynamics of thermoacoustic systems.

2.1 Model Components

In the following sections we discuss our modeling approaches for the physical standing wave engine depicted in Figure 2, including our development of a mathematical model and its corresponding optimization. We reduce our problem domain to two dimensions by taking advantage of the symmetry present in the stack. To account for the thermal behavior of the device, the reduced domain is given two constant temperature boundaries, one convective boundary, and one adiabatic boundary. In the thermal calculations, we are primarily interested in the temperature distribution achieved in the domain, and discuss several approaches to determine the relevant temperature profiles. Acoustically, we represent the stack's work flow and viscous resistance using expressions constructed from several structural variables, that are in turn involved in a number of structural constraints. The variables are the parameters[1]that we allow to be varied, while structural constraints are equations and inequalities that enforce restrictions on permissible variable combinations. We measure the quality of a given set of variable values that satisfies all of the constraints using an objective function.

Multiobjective optimization is concerned with the optimization of more than one objective function that are conflicting in nature Miettinen [1999]. They are conflicting in the sense that, if optimized individually, they do not share the same optimal solutions. When optimizing multiple objective components simultaneously, each objective is given a weight to allow the user to place desired emphasis. In this context, a Pareto optimal solution is one in which there does not exist another solution which strictly improves one of the considered objective components without worsening another objective component. Thus, by varying the weighted emphasis on objective components, multiple Pareto optimal solutions can be obtained and in turn be used to generate the efficient frontier.

2.1.1 Variables

We characterize the fundamental properties of the stack using the following five structural variables:

- L: Stack length,
- H: Stack height,
- Z: Stack placement,
- d_c: Channel diameter, and
- N: Number of channels.

Each variable has positive lower and upper bounds and is depicted in Figure 2. Both the stack length L and height H take real values between their bounds, where the stack height is defined as the radius of a cross section of the resonance tube. The placement of the stack in the axial direction of the resonator is modeled by continuous variable Z; near the closed end

[1]We differentiate between the terms *variables* and *parameters*, in that we use the term *variables* to indicate the structural components we allow to fluctuate in order to improve the objective, and the term *parameters* to indicate either known quantities (i.e., constants) or auxiliary quantities that are completely dependent on the values of the structural variables and other constant parameters.

of the resonance tube its value approaches 0 from above. We take the maximum length of the resonator tube to be a quarter-wavelength, i.e., $Z_{max} = \frac{\lambda}{4}$, implying that Z can effectively range from Z_{min} to $Z_{max} - L$ to properly account for the stack length. Because the geometry of the porous stack is based on the monolith structure used in experimentation Zink et al. [2009], we model it using square channels, representing the channel size with continuous variable d_c, so that the channel perimeter $\Pi_c = 4d_c$ and area $A_c = d_c^2$. We allow d_c to range from the thermal penetration depth δ_κ to $\mathcal{F}\delta_\kappa$, where $\mathcal{F}$ is an integer-valued multiplier on the thermal penetration depth. If the size of the stack's channels is too large, the key interaction between the gas and the wall does not occur, thus hindering the amplification of acoustic waves Swift [2002]; hence we take $\mathcal{F}$ to be 4 because it results in a channel dimension that still yields thermoacoustic performance. Finally, we model the number of channels N within the stack as an integer-valued variable.

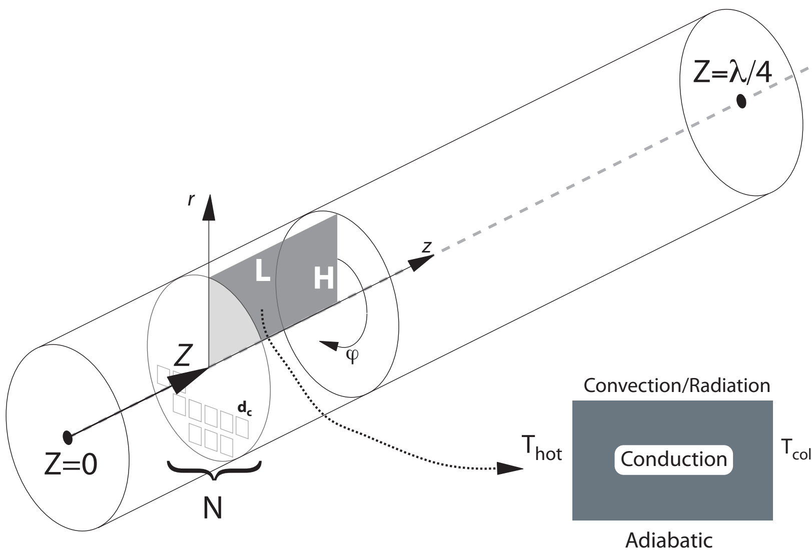

Figure 2: Computational domain and boundary conditions illustrating L, H, Z, N, d_c

2.1.2 Objectives

We consider multiple components in the objective function of our optimization model. Emphasizing power is prominent in the design of energy systems; this also justifies the optimization of the stack with regard to its viscous performance. We rely upon physical observations to provide justification with respect to thermal behavior. When one side of the stack is heated to approximately $300°C$ using about 50 W of electrical input, the temperature of the opposite side measures $50°C$. This temperature gradient yields a conductive heat flux that must be considered a loss. It is directly proportional to the stack's material (and thus thermal conductivity). We also account for the thermal losses through the shell of our thermoacoustic device. This is a less obvious source of loss in thermoacoustic devices, but must also be considered. Accounting for the dimensions and material properties of our small demonstrator engine, a cursory estimate of these losses is approximately 20 % of the total input power. This magnitude justifies our motivation to optimize the geometry of the stack to minimize the three aforementioned thermal losses.

Our final objective function is a combination of the following five individual components:

- W: Work output,
- R_ν: Viscous resistance,
- Q_{conv}: Convective heat flow,
- Q_{rad}: Radiative heat flow, and
- Q_{cond}: Conductive heat flow.

Each objective component has a weighting factor w_i to provide appropriate user-defined emphasis. The two acoustic objectives are the work output W of the thermoacoustic engine and the viscous resistance R_ν through the stack Swift [2002, 1988]. The thermal objectives include both the convective heat flow Q_{conv} and the radiative heat flow Q_{rad}, which we evaluate at the top boundary of the stack, as well as the conductive heat flow Q_{cond}, which is evaluated at the end of the resonance tube. Because work is the only objective to be maximized, we instead minimize its negative magnitude along with all of the other components.

As is typical in multiobjective optimization, the objective function components in our model are conflicting and of vastly different magnitudes and units. We can restore this imbalance by incorporating normalization factors on each component weight w_i. Thus, without loss of generality, we make the assumption that weights w_i are normalized in our following discussions, which makes each objective function component unitless and nonnegative in magnitude. Section 4.1 provides further details on our procedure to normalize the objective function components.

2.1.3 Structural Constraints

In addition to having lower and upper bounds, variables may only take values that satisfy certain physical properties governing the engine. One such property is that the total number of channels N of a given diameter d_c is limited by the cross-sectional radius of the resonance tube H. This relationship yields the constraint $\mathcal{A}N(d_c+t_w)^2 \leq \pi H^2$, where t_w represents the wall thickness around a single channel, and $\mathcal{A}$ represents the ratio of the area of a filled circle to its optimal packing by smaller square channels. From observations on optimal packings (see, e.g., Friedman), $1 \leq \mathcal{A} \leq 1.5$, so we set $\mathcal{A} = 1.25$. Other model constraints equate auxiliary parameters used in the optimization.

2.2 Mathematical Programming Formulation

We present our mathematical model (MPF) in this section. Taken together, expressions (2) – (27) represent a nonlinear mixed-integer program.

$$\text{(MPF)} \quad \min_{L,H,Z,d_c,N} \quad \zeta = w_1(-W) + w_2 R_\nu + w_3 Q_{conv} + w_4 Q_{rad} + w_5 Q_{cond} \tag{2}$$

subject to

$$\mathcal{A}N(d_c + t_w)^2 \leq \pi H^2, \tag{3}$$

$$W = \frac{\Pi_c \omega}{4}\left[\delta_\kappa \frac{(\gamma-1)p^2}{\rho c^2(1+\epsilon)}(\Gamma - 1) - \delta_\nu \rho u^2\right] LN = \omega \left[\delta_\kappa \frac{(\gamma-1)p^2}{\rho c^2(1+\epsilon)}(\Gamma - 1) - \delta_\nu \rho u^2\right] LNd_c, \tag{4}$$

$$R_\nu = \frac{\mu \Pi_c}{A_c^2 \delta_\nu}\frac{L}{N} = \frac{4\mu}{\delta_\nu}\frac{L}{Nd_c^3}, \tag{5}$$

$$Q_{conv} = H \int_0^{2\pi}\int_0^L h(T_s)\left(T_s - T_\infty\right) dz d\varphi, \tag{6}$$

$$Q_{rad} = H\ k_b \int_0^{2\pi}\int_0^L \epsilon\left(T_s^4 - T_\infty^4\right) dz d\varphi, \tag{7}$$

$$Q_{cond} = \int_0^{2\pi}\int_0^H \left(k_{rr}\frac{\partial T}{dr} + k_{zz}\frac{\partial T}{dz}\right) dr d\varphi, \tag{8}$$

$$Q_{cond}|_{z=L_{max}} = \int_0^{2\pi}\int_0^H \left(k_{zz}\frac{\partial T}{\partial z}\right) dr d\varphi. \tag{9}$$

Heat flow equations (6) – (9) depend on the following additional parameters:

$$h(T_s) = \frac{k_g}{2H} Nu, \tag{10}$$

$$Nu = 0.36 + \frac{0.518 Ra_D^{\frac{1}{4}}}{\left[1 + (\frac{0.559}{Pr})^{\frac{9}{16}}\right]^{\frac{4}{9}}}, \tag{11}$$

$$Ra_D = Gr\ Pr = \frac{g\beta(T_s - T_\infty)}{\nu\alpha}(2H)^3, \tag{12}$$

$$Pr = \frac{\nu}{\alpha}, \tag{13}$$

$$k_{rr} = \frac{k_s k_g (t_w + d_c)}{k_s t_w + k_g d_c}, \tag{14}$$

$$k_{zz} = \frac{k_s t_w + k_g d_c}{t_w + d_c}. \tag{15}$$

The work expression (4) depends on the following four parameters:

$$\epsilon = \frac{(\rho c_p \delta_\kappa)_g}{(\rho c_p \delta_s)_s}\frac{tanh\left((i+1)y_0/\delta_\kappa\right)}{tanh\left((i+1)l/\delta_s\right)}, \tag{16}$$

$$u_{max} = \frac{p_{max}}{\rho c}, \tag{17}$$

$$p = p_{max}\cos\left(\frac{2\pi Z}{\lambda}\right), \tag{18}$$

$$u = u_{max} \sin\left(\frac{2\pi Z}{\lambda}\right). \tag{19}$$

The variables are subject to the following restrictions:

$$L_{min} \leq L \leq L_{max}, \tag{20}$$

$$H_{min} \leq H \leq H_{max}, \tag{21}$$

$$\delta_\kappa \leq d_c \leq \mathcal{F}\delta_\kappa, \tag{22}$$

$$Z_{min} \leq Z \leq Z_{max} - L, \tag{23}$$

$$N_{min} \leq N \leq N_{max}, \tag{24}$$

$$L,\ H,\ Z,\ d_c \in\ \mathbb{R}_+; N \in\ \mathbb{Z}_+. \tag{25}$$

The following boundary conditions must also be enforced:

1. Constant hot side temperature (T_h),
2. Constant cold side temperature (T_c),
3. Adiabatic boundary, modeling the central axis of the cylindrical stack:
$$\left.\frac{\partial T}{dr}\right|_{r=0} = 0, \quad \text{and} \tag{26}$$
4. Free convection and radiation to surroundings (at T_∞) with temperature dependent heat transfer coefficient (h), emissivity (ε), and thermal conductivity (k):
$$k\left.\frac{\partial T}{dr}\right|_{r=H} = h\left(T_s - T_\infty\right) + \epsilon k_b\left(T_s^4 - T_\infty^4\right). \tag{27}$$

We denote by x the solution vector of structural variables, i.e., $x = [L, H, d_c, Z, N]$. Constraint (3) relates the channel diameter d_c and the number of possible channels N to the radius H of the cross-sectional area, while equations (4) – (8) express our five objective function components of interest. Equations (4) and (5) calculate the work W and viscous resistance R_ν, respectively, as functions of L, d_c, Z, and N (and indirectly H through (3)). Equations (6) – (9) represent heat flows. Equations (10) – (19) solve for parameters used in objective function components, (20) – (25) restrict variables values, and (26) – (27) represent heat flow boundary conditions. Note that u_{max} and p_{max} are related[2] at $z_o = 0$ as shown in (17).

Remark 1 *In equation (16), the real part of ϵ is observed to tend to $\frac{\sqrt{3}}{2}$, and we set ϵ to this value.*

Remark 2 *We set the hot-side temperature $T_h = \nabla T L + T_c$, where ∇T and T_c are predetermined values. Note that the constant temperature gradient ∇T is an approximation and its validity is assumed over the entire domain of structural variables (i.e., $L \in [L_{min}, L_{max}]$, $H \in [H_{min}, H_{max}]$, etc.). This behavior corresponds with experimental observations that clearly indicate a positive correlation between the stack length L and hot side temperature T_h in order to successfully sustain the thermoacoustic energy conversion. Additional details can be found in Section 2.3.1.*

Remark 3 *While the heat transfer coefficient h, in this case for natural convection, depends on the surface temperature T_s (a function of z), this value is calculated separately and treated as constant; see Section 2.3.2 for a related discussion.*

Remark 4 *We assume that constraint* (3) *is satisfied when variables H, N, and d_c are at their lower bounds, so that $\mathcal{A}N_{min}(d_{c_{min}} + t_w)^2 \leq \pi H_{min}^2$ holds.*

2.3 Approximating the Heat Flows

We next discuss how we arrived at equations (6) – (9), (26), and (27), including their approximation.

2.3.1 Estimating the Temperature Distribution

Given an input H (and L), it is necessary to find the solution of the 2D temperature distribution in our reduced domain, subject to boundary conditions detailed above. Due to the nature of the boundary conditions, the analytical solution is very difficult. Numerical solvers such as COMSOL Multiphysics COM [2005], MATLAB Finite Element Toolbox Mat [2007], etc. are another option to determine the temperature distribution. However, this precision comes at high computational cost. Considering that the temperature distribution is required for the estimation of the heat fluxes, only the temperature distribution at the shell surface and the temperature gradient at the cold side are of interest. For this purpose it is reasonable to reduce the temperature calculations to those two relevant values. The temperature distribution along the top surface can be well-approximated by an exponentially decaying temperature distribution throughout the domain. This behavior was determined through an analysis of the finite element solution. The final surface temperature distribution as a function of axial direction z is given by:

$$T_s = T_h e^{ln\left(\frac{T_c}{T_h}\right)\frac{z}{L}}. \tag{28}$$

This distribution is assumed to be valid on the surface characterized by $(z,\ r = H)$ and approximates the physical temperature distribution. This same temperature distribution is used to determine the axial temperature gradient at the cold side (required for the conductive heat flux). Considering again the rectangular domain, we can see that the temperature gradient in the center (i.e. bottom, $r = 0$) will vary linearly from T_h to T_c. Assuming that the temperature gradient at the cold side is exponential for all r will result in an underestimation of the conductive heat flux.

2.3.2 Determining the Heat Fluxes

The temperature distribution stated in equation (28) is then used to determine the convective and radiative heat transfer to the surroundings via:

$$Q_{conv} = 2\pi H h \int_0^L (T_s - T_\infty)\, dz. \tag{29}$$

[2] p_{max} is determined either by an informed choice based on domain knowledge, or via simulation.

As noted in Remark 3, the temperature dependent heat transfer coefficient $h(T)$ is determined in a preprocessor (derived from the appropriate Nusselt law, as stated in equation (11) and an average surface temperature), and is not considered as part of the integral. The radiative heat transfer (in the general case) is written as:

$$Q_{rad} = 2\pi H k_B \varepsilon \int_0^L \left(T_s^4 - T_\infty^4\right) dz, \tag{30}$$

which depends on the surface emissivity ε and Stefan-Boltzmann constant k_B, both of which are assumed to be independent of temperature.

After integrating we derive the following heat flow expressions:

$$Q_{conv} = 2\pi H L h \left[\frac{T_h}{ln\left(\frac{T_c}{T_h}\right)} \left(\frac{T_c}{T_h} - 1\right) - T_\infty \right], \quad \text{and} \tag{31}$$

$$Q_{rad} = 2\pi H L k_B \varepsilon \left[\frac{T_h^4 \left(e^{4ln\left(\frac{T_c}{T_h}\right)} - 1\right)}{4ln\left(\frac{T_c}{T_h}\right)} - T_\infty^4 \right]. \tag{32}$$

In the present case, this approximation of the temperature distribution (equation (28)) is also utilized to determine the conductive heat flow at $z = L$. The temperature distribution throughout the $2D$ domain implies that this estimate will fall between the extremes of:

1. the physical case (under anisotropic material properties and physical boundary conditions), and
2. the assumption of constant temperature gradient determined as $\frac{dT}{dz} = \frac{T_h - T_c}{L}$, as the latter case only exists at the adiabatic boundary $z,\ r = 0$ and quickly loses validity.

At the top surface $z,\ r = H$ the exponential distribution is assumed, so we determine the temperature gradient using this temperature distribution. Determining

$$\left.\frac{\partial T}{\partial z}\right|_{z=L} = \frac{T_c}{L} ln\left(\frac{T_c}{T_h}\right) \tag{33}$$

and implementing this in the general statement of the Fourier law of thermal conduction, we can express this heat flow as:

$$Q_{cond} = \frac{k_{zz}}{L} \pi H^2 T_c ln\left(\frac{T_h}{T_c}\right). \tag{34}$$

This expression for the conductive heat flow depends on the effective thermal conductivity in the z-direction as defined in equation (15). Using mild assumptions, equations (31), (32) and (34) give expressions for the heat flows that, while still nonlinear, no longer require external finite element solvers to evaluate.

3 Single Objective Optimization

We have presented a mathematical model that characterizes the essential elements of a standing wave thermoacoustic engine. Based on the discussion in Section 2.3.2, our nonlinear model can be solved independently of finite element solvers. In the following discussion we analyze restricted cases of our objectives, and identify general tendencies of the structural variables to influence individual objective components.

3.1 Acoustic Emphasis

The following two sections analyze the cases where objective function (2) is restricted to optimizing work and viscous resistance, respectively.

3.1.1 Emphasizing Work

Setting the objective function weights to $w_2 = w_3 = w_4 = w_5 = 0$ and $w_1 = 1$, the problem reduces to constraints (3), (4), (17) – (19), and variable restrictions (20) – (25). Objective function (2) becomes:

$$\min_{L,H,d_c,Z,N} \quad \zeta_W = (-W). \tag{35}$$

By incorporating (17) – (19) into the initial term of equation (4) (which is a function of Z through p and u), and defining $f_W(Z)$ as:

$$f_W(Z) = \omega \left[\delta_\kappa \frac{(\gamma - 1)\left[p_{max}\cos\left(\frac{2\pi Z}{\lambda}\right)\right]^2}{\rho c^2(1+\epsilon)}(\Gamma - 1) - \delta_\nu \rho \left[u_{max}\sin\left(\frac{2\pi Z}{\lambda}\right)\right]^2\right], \tag{36}$$

we can then express work as:

$$W = f_W(Z) L N d_c. \tag{37}$$

Because work W has a physically nonnegative interpretation, this implies $f_W(Z) \geq 0$, and because for our problem parameters $Z \leq \frac{\lambda}{4} - L$, it is favorable to set $Z^* = Z_{min}$. Also, because it appears nowhere else in the reduced problem, we set $L^* = L_{max}$. Regarding the remaining terms N and d_c, increasing either also improves the objective, but consumes limited resources as per constraint (3). Setting $H^* = H_{max}$ to allow both N and d_c to increase, equation (3) simplifies to:

$$\mathcal{A} N (d_c + t_w)^2 \leq \pi H_{max}^2. \tag{38}$$

Letting $c_W = -f_W(Z_{min})L_{max}$ and substituting equation (4) into (35) and rearranging gives:

$$\min_{d_c,N} \quad \zeta_W = c_W N d_c \tag{39}$$

subject to (22), (24), (25), and (38).

It follows from (22), (38) and (39) that d_c takes an upper bound of:

$$d_c = \min\left\{\mathcal{F}\delta_\kappa, \sqrt{\frac{\pi}{\mathcal{A}N}} H_{max} - t_w\right\}. \tag{40}$$

The first component of (40) is constant, and the second is monotonically decreasing in N. From (38) it also follows that:

$$N \leq \left\lfloor \frac{\pi H_{max}^2}{\mathcal{A}(d_c + t_w)^2} \right\rfloor, \tag{41}$$

so we define $N_{min} = 1$ and, because $\delta_\kappa \leq d_c$, we define $N_{max} = \left\lfloor \frac{\pi H_{max}^2}{\mathcal{A}(\delta_\kappa + t_w)^2} \right\rfloor$. Now considering the continuous value of N for which the two components in (40) are equal, let $\tilde{N} = \frac{\pi H_{max}^2}{\mathcal{A}(\mathcal{F}\delta_\kappa + t_w)^2}$. This leaves us with two cases:

1. for $N : N_{min} \leq N \leq \left\lfloor \tilde{N} \right\rfloor$, we have $d_c = \mathcal{F}\delta_\kappa$, and

2. for $N : \left\lceil \tilde{N} \right\rceil \leq N \leq N_{max}$, we have $d_c = \sqrt{\frac{\pi}{\mathcal{A}N}} H_{max} - t_w$.

Let us temporarily consider relaxing the integer restriction on N from (25), and let N_c take continuous values over the domain of N, i.e. $N_{min} \leq N_c \leq N_{max}$. Viewing the two cases above in light of N_c and (39) gives:

1. $\zeta_W = c_W N_c \mathcal{F}\delta_\kappa$ for $N_c : N_{min} \leq N_c \leq \tilde{N}$. Because $c_W < 0$, ζ_W is a monotonically decreasing function in terms of N_c, and so the optimal value of N_c over this domain is the largest value it can obtain, $N^* = \tilde{N}$.

2. $\zeta_W = c_W N_c \left(\sqrt{\frac{\pi}{\mathcal{A}N_c}} H_{max} - t_w \right)$ for $N_c : \tilde{N} \leq N_c \leq N_{max}$. For this case the first and second derivatives of ζ_W are, respectively:

$$\frac{d\zeta_W}{dN_c} = c_W \left[\sqrt{\frac{\pi}{4\mathcal{A}N_c}} H_{max} - t_w \right], \qquad \frac{d^2\zeta_W}{dN_c^2} = -c_W \sqrt{\frac{\pi}{16\mathcal{A}N_c^3}} H_{max}. \tag{42}$$

   Because $c_W < 0$, over the domain $N_c : \tilde{N} \leq N_c \leq N_{max}$ the second derivative of $\zeta_W > 0$, implying convexity of ζ_W and so ζ_W has a single global minimum. Setting the first derivative in (42) equal to zero and solving, the minimal value of ζ_W occurs at $N_c = \frac{\pi H_{max}^2}{4\mathcal{A}t_w^2}$. Because of the convexity of ζ_W in this region, then if $\tilde{N} \leq \frac{\pi H_{max}^2}{4\mathcal{A}t_w^2} \leq N_{max}$, we have $N_c^* = \frac{\pi H_{max}^2}{4\mathcal{A}t_w^2}$. Otherwise, $\tilde{N} > \frac{\pi H_{max}^2}{4\mathcal{A}t_w^2}$, and in this case ζ_W is increasing on the interval $\left[\tilde{N}, N_{max}\right]$, and so $N_c^* = \tilde{N}$.

In light of the previous two cases, to ensure $N \in \mathbb{Z}_+$ we have:

$$N^* \in \left\{ \left\lfloor \tilde{N} \right\rfloor, \left\lceil \tilde{N} \right\rceil, \left\lfloor \frac{\pi H_{max}^2}{4\mathcal{A}t_w^2} \right\rfloor, \left\lceil \frac{\pi H_{max}^2}{4\mathcal{A}t_w^2} \right\rceil \right\}; \quad d_c^* = \begin{cases} \mathcal{F}\delta_\kappa & \text{if } N^* = \left\lfloor \tilde{N} \right\rfloor; \\ \sqrt{\frac{\pi}{\mathcal{A}N^*}} H_{max} - t_w & \text{otherwise.} \end{cases} \tag{43}$$

We then choose from (43) the values of N and corresponding d_c that minimize (39). Based upon our problem data (see Section 7), a global optimum that minimizes ζ_W is:

$$x^* = \left[L_{max}, H_{max}, \sqrt{\frac{\pi}{\mathcal{A}N^*}} H_{max} - t_w, Z_{min}, \left\lceil \frac{\pi H_{max}^2}{4\mathcal{A}t_w^2} \right\rceil \right].$$

Figure 3 plots ζ_W as a function of N; the value of $N^* = \left\lceil \frac{\pi H_{max}^2}{4\mathcal{A}t_w^2} \right\rceil$ minimizing ζ_W is apparent.

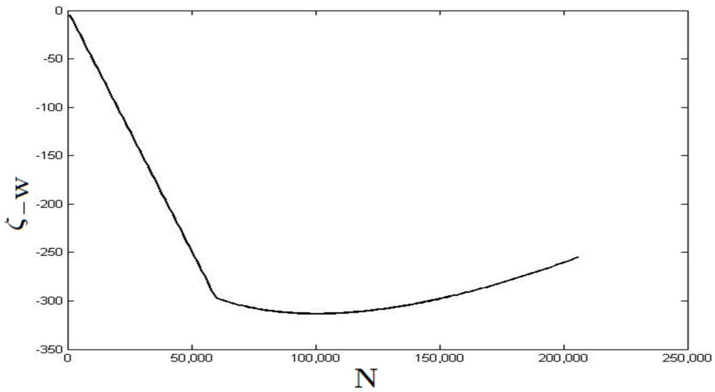

Figure 3: ζ_W plotted as function of N and showing minimum

This optimal solution can be physically interpreted as making the stack as long and wide as possible ($L^* = L_{max}$ and $H^* = H_{max}$), and also increasing the number of channels N and the channel diameter d_c so that we maximize the thermoacoustically active surface area. Moving the stack as near as possible to the closed end ($Z^* = Z_{min}$) maximizes the available pressure amplitude for the thermodynamic cycle and thus work output W.

3.1.2 Emphasizing Viscous Resistance

We emphasize R_ν by setting objective function weights $w_1 = w_3 = w_4 = w_5 = 0$ and $w_2 = 1$. The problem then simplifies to constraints (3), (5), and variable restrictions (20) – (25). Objective function (2) becomes:

$$\min_{L,H,d_c,Z,N} \quad \zeta_{R_\nu} = R_\nu. \tag{44}$$

Set Z^* to any value between its lower and upper bounds, e.g. $Z^* = Z_{min}$, and set $L^* = L_{min}$. N and d_c are constrained by (3); setting $H^* = H_{max}$ affords the greatest flexibility for N and d_c to increase. Let $c_{R_\nu} = \frac{4\mu L_{min}}{\delta_\nu}$, then (44) can be rewritten as:

$$\min_{d_c,N} \quad \zeta_{R_\nu} = \frac{c_{R_\nu}}{N d_c^3} \tag{45}$$

subject to (3), (24), (22), and (25). Much of the discussion in Section 3.1.1 concerning d_c still holds, e.g. equations (38), (40) and (41). Maintaining our definition of $\tilde{N}$, the following two cases remain:

1. for $N : N_{min} \leq N \leq \left\lfloor \tilde{N} \right\rfloor$, we have $d_c = \mathcal{F}\delta_\kappa$, and
2. for $N : \left\lceil \tilde{N} \right\rceil \leq N \leq N_{max}$, we have $d_c = \sqrt{\frac{\pi}{\mathcal{A}N}} H_{max} - t_w$.

Instead of minimizing ζ_{R_ν} as in (45), let us instead maximize $\overline{\zeta}_{R_\nu} = N d_c^3$, as the optimal values of N^* and d_c^* are identical. As in Section 3.1.1 we temporarily consider relaxing the integer restriction on N from (25), allowing N_c to take continuous values over the domain of N, i.e. $N_{min} \leq N_c \leq N_{max}$. Viewing these two cases in light of N_c and $\overline{\zeta}_{R_\nu}$ gives:

1. $\overline{\zeta}_{R_\nu} = N_c(\mathcal{F}\delta_\kappa)^3$ for $N_c : N_{min} \leq N_c \leq \tilde{N}$.

   Here, $\overline{\zeta}_{R_\nu}$ is a monotonically increasing function in terms of N_c, and so the optimal value of N_c over this domain is the largest value it can obtain, $\tilde{N}$.

2. $\overline{\zeta}_{R_\nu} = N_c \left(\sqrt{\frac{\pi}{\mathcal{A} N_c}} H_{max} - t_w \right)^3$ for $N_c : \tilde{N} \leq N_c \leq N_{max}$.

   Over this interval, differentiating $\overline{\zeta}_{R_\nu}$ gives:

$$\frac{d\overline{\zeta}_{R_\nu}}{dN_c} = \frac{3t_w^2}{2} \left(\frac{\pi}{\mathcal{A}} H_{max}^2 \right)^{\frac{1}{2}} N_c^{-\frac{1}{2}} - \frac{1}{2} \left(\frac{\pi}{\mathcal{A}} H_{max}^2 \right)^{\frac{3}{2}} N_c^{-\frac{3}{2}} - t_w^3, \tag{46}$$

   and upon a second differentiation, we obtain:

$$\frac{d^2\overline{\zeta}_{R_\nu}}{dN_c^2} = \frac{3}{4} \left(\frac{\pi}{\mathcal{A}} H_{max}^2 \right)^{\frac{3}{2}} N_c^{-\frac{5}{2}} - \frac{3t_w^2}{4} \left(\frac{\pi}{\mathcal{A}} H_{max}^2 \right)^{\frac{1}{2}} N_c^{-\frac{3}{2}}. \tag{47}$$

   The second derivative of $\overline{\zeta}_{R_\nu} > 0$ over the entire domain $N_c : \tilde{N} < N_c \leq N_{max}$, implying $\overline{\zeta}_{R_\nu}$ is convex. Thus the maximum over this domain occurs at one of the endpoints of the interval, i.e., $N_c^* \in \left\{ \tilde{N}, N_{max} \right\}$.

From these two cases, and because $N \in \mathbb{Z}_+$ we have:

$$N^* \in \left\{ \left\lfloor \tilde{N} \right\rfloor, \left\lceil \tilde{N} \right\rceil, N_{max} \right\}; \quad d_c^* = \begin{cases} \mathcal{F}\delta_\kappa & \text{if } N^* = \left\lfloor \tilde{N} \right\rfloor; \\ \sqrt{\frac{\pi}{\mathcal{A}N^*}} H_{max} - t_w & \text{otherwise.} \end{cases} \tag{48}$$

We then choose from (48) the values of N and corresponding d_c that minimize (45). For our specific problem parameters, a global minimizer for ζ_{R_ν} is:

$$x^* = \left[L_{min}, H_{max}, \mathcal{F}\delta_\kappa, Z_{min}, \left\lfloor \tilde{N} \right\rfloor \right].$$

Figure 4 plots ζ_{R_ν} as a function of N; the value of $N^* = \left\lfloor \tilde{N} \right\rfloor = \left\lfloor \frac{\pi H_{max}^2}{\mathcal{A}(\mathcal{F}\delta_\kappa + t_w)^2} \right\rfloor$ minimizing ζ_{R_ν} is apparent.

Physically, this result can be interpreted as reducing the individual (viscous) resistance of each channel to its minimum by decreasing their length ($L^* = L_{min}$) and then bundling as many of those small resistances in parallel to further decrease the net resistance. This is illustrated by the addition of the respective inverse resistances to determine a net resistance when arranged in parallel:

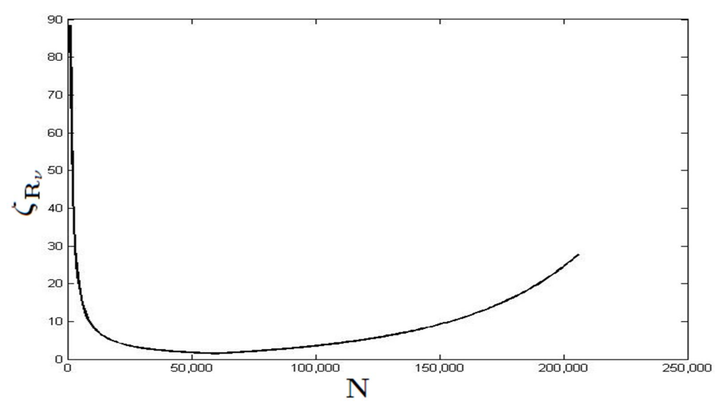

Figure 4: ζ_{R_ν} plotted as function of N and showing minimum

$$R_{net} = \left[\sum_{i=1}^{N} \frac{1}{R_i} \right]^{-1}. \tag{49}$$

In the case where all R_i have the same value, this equation reduces to $R_{net} = \frac{R_i}{N}$, indicating the increasing behavior of N to achieve minimum resistance.

3.2 Thermal Emphasis

We have thus far considered how acoustic objectives W and R_ν are affected by changes in the structural variables. We next discuss the individual thermal objectives by isolating each heat flow objective function component.

3.2.1 Emphasizing Convective, Radiative Heat Fluxes

We can emphasize Q_{conv} by setting objective function weights $w_1 = w_2 = w_4 = w_5 = 0$ and $w_3 = 1$. The problem then reduces to constraints (3), (10) – (13), variable restrictions (20) – (25), and expression (31). Alternatively, we can emphasize Q_{rad} by setting objective function weights $w_1 = w_2 = w_3 = w_5 = 0$ and $w_4 = 1$, so that only constraints (3), (16), variable restrictions (20) – (25), and (32) are active. For these restricted optimization problems, objective function (2) becomes, respectively:

$$\min_{L,H,d_c,Z,N} \quad \zeta_{Q_{conv}} = Q_{conv}; \quad \min_{L,H,d_c,Z,N} \quad \zeta_{Q_{rad}} = Q_{rad}. \tag{50}$$

Neither of these restricted models are dependent on Z, so Z^* can be set to any value between its lower and upper bounds (note our assumption that h is not dependent on Z in Remark 3). Considering H, for Q_{cond} it can be shown from equations (10) – (13) that h is proportional to $H^{-1/4}$. Because the resulting exponent on the H variable remains positive in equation (31), it is still desirable to set $H^* = H_{min}$. For Q_{rad} we also set H to $H^* = H_{min}$ based on (32). Setting $N^* = N_{min}$ and $d_c^* = d_{c_{min}}$ ensures that H can take its minimum value in constraint (3) (see assumption in Remark 4).

A global optimum minimizing both $\zeta_{Q_{conv}}$ and $\zeta_{Q_{rad}}$ is $x^* = [L_{min}, H_{min}, d_{c_{min}}, Z_{min}, N_{min}]$. For Q_{cond}, this optimum minimizes the surface area and limits the temperature range in the stack, thereby minimizing the convective heat flow. Similarly for Q_{rad}, this optimum lowers driving potential and surface area to minimize radiative heat flow.

3.2.2 Emphasizing Conductive Heat Flux

We emphasize Q_{cond} by setting objective function weights $w_1 = w_2 = w_3 = w_4 = 0$ and $w_5 = 1$, so that only constraints (3), (15), variable restrictions (20) – (25), and (34) are active. Objective function (2) becomes:

$$\min_{L,H,d_c,Z,N} \quad \zeta_{Q_{cond}} = Q_{cond}. \tag{51}$$

Similar to previous sections, this model is not dependent on Z, so that Z^* can be set to any value between its lower and upper bounds. Equation (15) can be rearranged as:

$$k_{zz} = k_g + \frac{t_w(k_s - k_g)}{(t_w + d_c)}, \tag{52}$$

and so merging (52) with (34) and rearranging gives:

$$Q_{cond} = \pi T_c \left[k_g + \frac{t_w(k_s - k_g)}{(t_w + d_c)} \right] \frac{ln\,(\nabla T L + T_c) - ln\,(T_c)}{L} H^2. \tag{53}$$

The expression $\frac{ln(\nabla TL+T_c)-ln(T_c)}{L}$ is always positive, so setting L^* to L_{max} decreases Q_{cond}, improving (51). We can also improve Q_{cond} by both decreasing H and increasing d_c. However, there is tension in constraint (3) between decreasing H and increasing d_c. Because N appears only on the left-hand side of (3) in this restricted model, we can set $N^* = N_{min} = 1$ to allow d_c and H the most flexibility. Letting $c_{Q1} = \pi T_c k_g \frac{ln(\nabla TL_{max}+T_c)-ln(T_c)}{L_{max}}$ and $c_{Q2} = \pi T_c\left[t_w(k_s-k_g)\right]\frac{ln(\nabla TL_{max}+T_c)-ln(T_c)}{L_{max}}$, and noting both are positive, then substituting these into (53) and (51) gives the following optimization problem over two continuous variables:

$$\min_{H,d_c} \quad \zeta_{Q_{cond}} = c_{Q1}H^2 + c_{Q2}\frac{H^2}{(t_w+d_c)} \tag{54}$$

subject to constraint (3) and variable restrictions (21), (22), and (25).

Given any fixed value for H, it follows from our discussions and (3) that d_c will take the value of:

$$d_c = \min\left\{\mathcal{F}\delta_\kappa, \sqrt{\frac{\pi}{\mathcal{A}}}H - t_w\right\}. \tag{55}$$

Let $\tilde{H} = \frac{\mathcal{F}\delta_\kappa + t_w}{\sqrt{\frac{\pi}{\mathcal{A}}}}$ be the value of H for which the value of d_c transitions in (55). This leaves us with two cases:

1. for $H : H_{min} \le H \le \tilde{H}$, we have $d_c = \sqrt{\frac{\pi}{\mathcal{A}}}H - t_w$, and
2. for $H : \tilde{H} \le H \le H_{max}$, we have $d_c = \mathcal{F}\delta_\kappa$.

For both intervals $\zeta_{Q_{cond}}$ is nondecreasing, so that $H^* = H_{min}$, implying $d_c^* = \sqrt{\frac{\pi}{\mathcal{A}}}H_{min} - t_w$. Thus a global optimum minimizing $\zeta_{Q_{cond}}$ is $x^* = \left[L_{max}, H_{min}, \sqrt{\frac{\pi}{\mathcal{A}}}H_{min} - t_w, Z_{min}, N_{min}\right]$.

The physical interpretation of these results indicates that minimizing the conductive heat flow yields a different solution than that of the convective and radiative heat flows. The channel design is a function of gas and solid thermal conductivity, and takes an optimal value between its upper and lower bounds. For an actual engine design this information may be useful in designing stacks that require the least amount of cooling for a given (heat) power input.

3.3 Single Objective Optima: Variable Analysis

Table 1 summarizes the results of Sections 3.1 and 3.2. It highlights the behavior of the structural variables, along the left, when individually optimizing the five objective function components that appear across the top of the table. For these objectives, $\uparrow$ indicates an increasing tendency, $\downarrow$ indicates a decreasing tendency, and $\longleftrightarrow$ indicates no impact, while †indicates there is conflicting tension between variables. ‡indicates that Z can be set to Z_{min} in all cases, as only objective W depends on it, and decreasing it improves this objective while having no effect on the other objectives (based on our assumption in Remark 3). Also note the lack of tension in variables for the Q_{conv} and Q_{rad} heat flows, which share the same optimal solution.

Table 1: Optimizing individual objective components: structural variable tendencies

	$(-)W$	R_ν	Q_{conv}	Q_{rad}	Q_{cond}
L	$\uparrow$	$\downarrow$	$\downarrow$	$\downarrow$	$\uparrow$
H	$\uparrow$	$\uparrow$	$\downarrow$	$\downarrow$	$\downarrow$
d_c	$\uparrow^\dagger$	$\uparrow^\dagger$	$\downarrow$	$\downarrow$	$\uparrow$
Z	$\downarrow^\ddagger$	$\longleftrightarrow$	$\longleftrightarrow$	$\longleftrightarrow$	$\longleftrightarrow$
N	$\uparrow^\dagger$	$\uparrow^\dagger$	$\downarrow$	$\downarrow$	$\downarrow$

4 Multiobjective Optimization

In Section 3 we examine optimization over every individual component of objective function (2), providing analytical solutions that do not require computational solution methods to identify global optima. In this section we consider multiple objective components simultaneously, and suggest straightforward algorithmic approaches to identify optimal solutions for these cases. Before proceeding, we first discuss our approach to ensure objective function weights are normalized, which is necessary whenever more than one objective function component is considered.

4.1 Normalizing Objective Function Components

When multiple objective function components are given nonzero weights, objective function (2) of (MPF) can have a predisposed bias towards those components having larger magnitudes, and unit discrepancies across the various objective components create further complications. These issues can be simultaneously addressed for each objective component by obtaining a normalization factor to offset any disparate magnitudes and eliminate inconsistent units.

Our proposed normalization approach is based on a method described in Grodzevich and Romanko [2006]. Let a set $\mathcal{I}$ of objective components of interest from objective (2) be indexed by $i \in \mathcal{I}$. As (MPF) contains five objective components, $|\mathcal{I}| \leq 5$. Then for all indices $j \notin \mathcal{I}$, we set $w_j = 0$. For normalization coefficients n_i the approach uses the differences of values between certain *Utopia* and *Nadir* vectors that are of the same dimension as the number of considered objective function components $|\mathcal{I}|$, and are formed using information obtained from independent optimization of each objective function component.

The *Utopia* vector $\mathcal{U}$ is created as follows. For each $i \in \mathcal{I}$, we set $w_i = 1$ and $w_k = 0 \ \forall \ k \in \mathcal{I} : k \neq i$. Let $\mathcal{G}_i$ be the selected objective component. Optimizing the resulting reduced problem generates optimal objective function value $\mathcal{G}_i^*$ and optimal solution $x_i^* = [L_i^*, H_i^*, d_{c_i}^*, Z_i^*, N_i^*]$. Then $\mathcal{U}_i = \mathcal{G}_i^*$. After repeating this process for all $i \in \mathcal{I}$, the *Nadir* vector $\mathcal{N}$ makes use of the optimal solutions x_i^* from these optimizations, evaluating each x_i^* in the respective individual objective functions $\mathcal{G}_i^*$ over all $i \in \mathcal{I}$ to find its worst value. Thus, the Nadir vector is constructed as $\mathcal{N}_i = \max\limits_{\ell=1,\ldots,5} \{\mathcal{G}_i(x_\ell^*)\} \ \forall \ i \in \mathcal{I}$.

For each $i \in \mathcal{I}$, the differences $\mathcal{N}_i - \mathcal{U}_i$ provide the length of interval over which the optimal objective functions vary within the set of optimal solutions; note that these differences are always non-negative. They are used to construct the normalization factors n_i as:

$$n_i = \frac{1}{\mathcal{N}_i - \mathcal{U}_i}. \tag{56}$$

For instance, if we consider for $\mathcal{I}$ all five of the objective components of objective function (2), then it can be normalized as:

$$w_1 n_1((-W) - \mathcal{U}_1) + w_2 n_2(R_\nu - \mathcal{U}_2) + w_3 n_3(Q_{conv} - \mathcal{U}_3) + w_4 n_4(Q_{rad} - \mathcal{U}_4) + w_5 n_5(Q_{cond} - \mathcal{U}_5). \tag{57}$$

We use this normalization scheme for all cases involving multiple objective function components. Note that the Utopia values are subtracted from every component so to ensure that the term is unitless and nonnegative, thereby eliminating any bias of magnitude.

4.2 Emphasizing Work and Viscous Resistance

We can simultaneously optimize the acoustic objectives W and R_ν by assigning objective weights $w_3 = w_4 = w_5 = 0$ with $w_1 > 0$, $w_2 > 0$. Then (MPF) reduces to constraints (3), (4), (17) – (19) and variable restrictions (20) – (25). Objective function (2) reduces to:

$$\min_{L,H,d_c,Z,N} \quad \zeta_{Acoustic} = w_1(-W) + w_2 R_\nu. \tag{58}$$

With respect to (36), let $\overline{c}_W = -w_1 f_W(Z_{min})$ and $\overline{c}_{R_\nu} = w_2 \frac{4\mu}{\delta_\nu}$, so that $\overline{c}_W$ and $\overline{c}_{R_\nu}$ are, respectively, the constant terms from Sections 3.1.1 and 3.1.2 without fixing L. Setting $Z^* = Z_{min}$ and $H^* = H_{max}$ as in Sections 3.1.1 and 3.1.2, and substituting $\overline{c}_W$, $\overline{c}_{R_\nu}$, W and R_ν into objective function (58) gives:

$$\min_{L,N,d_c} \quad \zeta_{Acoustic} = \left(\overline{c}_W N d_c + \frac{\overline{c}_{R_\nu}}{N d_c^3} \right) L \tag{59}$$

subject to (20), (24), (22), (25), and (38). The tradeoffs between variables L, N and d_c can be investigated by first fixing N to $\overline{N} \in [N_{min}, N_{max}] \cap \mathbb{Z}$, then using $\overline{N}$ in equation (40) to fix d_c to $\overline{d_c} = \min \left\{ \mathcal{F}\delta_\kappa, \sqrt{\frac{\pi}{\mathcal{A}\overline{N}}} H_{max} - t_w \right\}$. Depending on the sign of the resulting coefficient on L in (59), L can be set to:

$$\overline{L} = \begin{cases} L_{min} & \text{if } \left(\overline{c}_W \overline{N}\ \overline{d_c} + \frac{\overline{c}_{R_\nu}}{\overline{N}\ \overline{d_c}^3} \right) \ \geq \ 0; \\ L_{max} & \text{otherwise.} \end{cases} \tag{60}$$

Thus for every fixed $\overline{N}$ the problem has a fixed value of $\overline{d_c}$ and $\overline{L}$. The optimal levels of L^*, N^* and d_c^* can be found by enumerating over all values $\overline{N} \in [N_{min}, N_{max}] \cap \mathbb{Z}$. We implement such an approach in MATLAB Mat [2007], which takes at most a few minutes to solve on a Windows XP machine equipped with a 2.16GHz Intel Core 2 processor and 2GB of RAM.

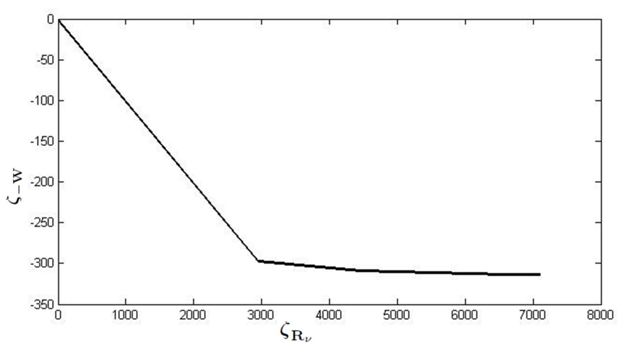

Figure 5: Simultaneously minimizing $-W$ and R_ν

By iterating over multiple sets of objective function weights w_1 and w_2, the frontier of efficient points can be generated that optimize the respective acoustic objectives. This acoustic frontier is partially illustrated in Figure 5.

Maximizing the radius of the stack ($H^* = H_{max}$) both maximizes the work by allowing many channels N while simultaneously reducing the viscous resistance (as per discussion in Section 3.1.2). Also from the discussion in Sections 3.1.1 and 3.1.2, depending on the weighting of w_1 and w_2, the optimal length L is either its upper or lower bound. Moving the stack nearer to the closed end ($Z^* = Z_{min}$) increases the available pressure amplitude for the thermodynamic cycle that increases work output W without affecting R_ν.

4.3 Emphasizing All Objective Components

Lastly, we simultaneously consider all five objective components by regarding work W and viscous resistance R_ν as two distinct objective components, and representing heat with a third distinct objective component Q_{all}, defined as the sum of the three heat components Q_{conv}, Q_{rad}, and Q_{cond}. We use three weights, w_W, w_{R_ν} and $w_{Q_{all}}$, and divide $w_{Q_{all}}$ equally among the three heat components comprising Q_{all}.

As in Section 4.2, we propose to determine the frontier of efficient points that optimize the three weighted objectives W, R_ν, and Q_{all} by iterating over multiple values of objective function weights w_W, w_{R_ν} and $w_{Q_{all}}$. However, due to the lack of a closed form solution over the considered objective function components, this requires a global optimization approach to identify optimal solutions.

For fixed values of w_W, w_{R_ν} and $w_{Q_{all}}$, we call the global optimization routine DIRECT Perttunen et al. [1993], a derivative free algorithm based on Lipschitzian optimization with proven finite convergence. The algorithm begins by constructing a hyper-rectangle that contains the original (continuous) variable space, and progressively improves the objective by repeatedly sub-dividing hyper-rectangles as it moves toward the global optimum. The particular implementation we use is due to Finkel Finkel [2003], and coded in MATLAB.

This process generates optimal solutions corresponding to various sets of weights w_W, w_{R_ν} and $w_{Q_{all}}$. These optimal solutions are then used to construct the efficient frontier of optimal solutions, which is partially illustrated in the three-dimensional objective space by the fitted surface appearing in Figures 6(a) and 6(b). The conflicting nature of the three objectives can be observed in both profiles, with each competing objective on respective axes. Figure 6(a) provides a side profile of the efficient frontier, where the bottom left corner is improving for all three objectives, and illustrates how an improvement in a single objective component causes the remaining two objectives to worsen. Figure 6(b) depicts the same phenomenon from a top profile, where the rear corner is improving for every objective.

5 Conclusions

We demonstrate how optimization techniques can improve the design of thermoacoustic devices. Previous studies have largely relied upon parametric studies. In contrast to these, where only one parameter is varied while all others are kept constant, we propose a mathematical model that simultaneously optimizes multiple variables over a set of constraints, and includes an objective function quantifying both acoustic and thermal performance.

We analyze cases of single objective components (two acoustic and three thermal), as well as two cases of multiobjective optimization. For the single objective cases, we identify analytical solutions, while for the cases of multiple objectives, we generate the efficient frontier of optimal solutions for various objective weights. For both cases (the single objective as well as multiple objective approach), we show that there are non-trivial solutions to each design that have the potential to improve the energetic performance of thermoacoustic devices. The approach presented here still allows for a large amount of personal preference, i.e. emphasis on purely acoustic performance or purely thermal performance, or any given blend of the two main groups of objectives.

An alternative way to simultaneously maximize work and minimize losses (viscous resistance as well as heat flows) is to consider the thermal efficiency η, which can be defined as the ratio of the work output over the sum of the work output and losses. Thus we can consider the following optimization problem:

$$\max \ \frac{W}{W + \tilde{w_2}R_v + \tilde{w_3}Q_{conv} + \tilde{w_4}Q_{rad} + \tilde{w_5}Q_{cond}} \tag{61}$$

subject to the original constraints of (MPF). This results in a mixed-integer fractional programming problem, the numerator of which represents the work output, and the denominator being a sum of the work and combined (viscous and thermal) losses.

One way to solve fractional programs is via Dinkelbach's algorithm Dinkelbach [1967]. Briefly, Dinkelbach's algorithm eliminates the ratio in objective (61) by instead considering a sequence of problems that parameterize (61) with:

$$\eta = \frac{W}{W + \tilde{w_2}R_v + \tilde{w_3}Q_{conv} + \tilde{w_4}Q_{rad} + \tilde{w_5}Q_{cond}}, \tag{62}$$

and replace objective function (61) by:

$$\max \ W - \eta(W + \tilde{w_2}R_v + \tilde{w_3}Q_{conv} + \tilde{w_4}Q_{rad} + \tilde{w_5}Q_{cond}). \tag{63}$$

Dinkelbach's algorithm optimizes (63) subject to the original (MPF) constraints, iteratively updating its choice of η in order to identify η^* for which the maximum value of (63) equals zero. The sequence of choices for η finitely converge to η^*, solving the alternative representation and thus the original problem as well. Note the equivalence between the version of (MPF) as described in Section 4.3, and that of a single instance of (63) (corresponding to a fixed value of η) subject to the constraints in (MPF). Therefore solving (61) can be reduced to iteratively applying our procedure until the maximum of (63) attains zero.

6 Acknowledgements

The authors thank two anonymous referees whose constructive comments substantially improved this manuscript. Andrew C. Trapp was supported by the US Department of Education Graduate Assistance in Areas of National Need (GAANN) Fellowship Program grant P200A060149, administered through the Mascaro Center for Sustainable Innovation at the University of Pittsburgh. Laura Schaefer was supported by NSF grant CBET-0729905.

7 Nomenclature

A	Area (m^2)
c	Speed of sound ($m \cdot s^{-1}$)
C	Capacitance (m^{-1})
c_p	Heat capacity ($J \cdot kg^{-1} \cdot K^{-1}$)
d	Diameter
D	Dimension
f	Frequency (s^{-1})
g	Gravitational acceleration
h	Heat transfer coefficient ($W \cdot m^{-2} \cdot K^{-1}$)
H	Height (Cylindrical Radius) (m)
k_b	Boltzmann constant
k	Thermal conductivity ($W \cdot m^{-1} \cdot K^{-1}$)
l	Plate thickness (m)
L	Inertance ($kg \cdot m^{-4}$), length (m)
p	Pressure ($N \cdot m^{-2}$)
$\tilde{p}$	Constant for quadratic pressure estimate
Q	Heat flow (W)
r	Variable radius height (m) along radial direction
$\tilde{r}$	Constant for viscous resistance formulation
R	Resistance ($kg \cdot m^{-2} \cdot s^{-1}$)
T	Temperature (K, $°C$)
u	Velocity ($m \cdot s^{-1}$)
$\tilde{u}$	Constant for quadratic velocity estimate
w	Objective function component weight
W	Acoustic work (W) per channel
y	Plate spacing (m)
z	Local variable, refers to distance along the stack, 0 at "hot side" of stack
Z	Stack Placement (along z axis), 0 at closed end

Greek Symbols

α	Thermal diffusion rate ($m^2 \cdot s^{-1}$)
β	Thermal expansion coefficient (taken as $1/T_\infty$)
δ	Penetration depth (m)
ϵ	Plate heat capacity ratio
ε	Surface emissivity
γ	Isentropic coefficient
Γ	Temperature gradient ratio
λ	Wavelength
μ	Dynamic viscosity ($kg \cdot m^{-1} \cdot s^{-1}$)
ν	Viscous diffusion rate ($m^2 \cdot s^{-1}$)
ρ	Density ($kg \cdot m^{-3}$)
ω	Angular frequency (s^{-1})
Π	Perimeter (m)
∇T	Temperature gradient ($K \cdot m^{-1}$)

Dimensionless Groups

$\mathcal{A}$	Packing Number ($\approx 1.25 \pm 0.25$)
$\mathcal{F}$	Fixed Upper Bounding Constant (4)
Gr	Grasshoff Number
Nu	Nusselt Number
Pr	Prandtl Number
Ra	Rayleigh Number

Subscripts and Superscripts

o	Naught
∞	Ambient, free stream
c	Channel, cold
$char$	Characteristic
$crit$	Critical
$cond$	Conductive
$conv$	Convective
D	Diameter
h	Hot side
κ	Thermal
m	Time averaged
obj	Objective
rad	Radiative
s	Solid, surface, stable
rr,rz,zr,zz	Tensor directions
ν	Viscous
w	Wall

References

Scott Backhaus and Greg W. Swift. A thermoacoustic Stirling heat engine: Detailed study. *Journal of the Acoustical Society of America*, 107(6):3148–66, 2000.

Kevin J. Bastyr and Robert M. Keolian. High-frequency thermoacoustic-Stirling heat engine demonstration device. *Acoustics Research Letters Online*, 4(2):37–40, 2003.

Etienne Besnoin. *Numerical Study of Thermoacoustic Heat Exchangers*. PhD thesis, Johns Hopkins University, 2001.

Peter H. Ceperley. Gain and efficiency of a short traveling wave heat engine. *Journal of the Acoustical Society of America*, 77(3):1239–1244, 1985.

Comsol Multiphysics Users Guide. COMSOL AB, Burlington, MA, USA, 2005.

W. Dinkelbach. On non-linear fractional programming. *Management Science*, 13(7):492–498, 1967.

Daniel E. Finkel. *DIRECT Optimization Algorithm User Guide*. Center for Research in Scientific Computation, North Carolina State University, Raleigh, NC 27695-8205, March 2003.

Erich Friedman. http://www2.stetson.edu/˜efriedma/squincir/.

Steven L. Garrett. Reinventing the engine. *Nature*, 339:303–305, 1999.

Steven L. Garrett. The power of sound. *American Scientist*, 88(6):516–526, 2000.

O. Grodzevich and O. Romanko. Normalization and other topics in multiobjective optimization. In *Proceedings of the First Fields-MITACS Industrial Problems Workshop*, pages 89–102. The Fields Institute, 2006.

Cila Herman and Z Travnicek. Cool sound: The future of refrigeration? Thermodynamic and heat transfer issues in thermoacoustic refrigeration. *Heat and Mass Transfer*, 42: 492–500, 2006.

Noboru Kagawa. *Regenerative Thermal Machines*. International Institute for Refrigeration, Paris, 2000.

S C. Kaushik and S Kumar. Finite time thermodynamic analysis of endoreversible Stirling heat engine with regenerative losses. *Energy*, 25:989–1003, 2000.

MATLAB User's Guide. The MathWorks, Inc., 2007.

K. Miettinen. *Nonlinear multiobjective optimization*. Springer, 1999.

Brian L. Minner, James E. Braun, and Luc G. Mongeau. Theoretical evaluation of the optimal performance of a thermoacoustic refrigerator. In *ASHRAE Transactions: Symposia*, volume 103, pages 873–887, 1997.

C. D. Perttunen, D. R. Jones, and B. E. Stuckman. Lipschitzian optimization without the lipschitz constant. *Journal of Optimization Theory and Application*, 79(1):157–181, 1993.

Matthew E. Poese, Robert W.M. Smith, Steven L. Garrett, Rene van Gerwen, and Pete Gosselin. Thermoacoustic refrigeration for ice cream sales. In *Proceedings of the 6^{th} IIR Gustav Lorentzen Conference*, 2004.

Greg W. Swift. Thermoacoustic engines. *Journal of the Acoustical Society of America*, 84 (4):1145–1180, 1988.

Greg W. Swift. *Thermoacoustics: A unifying perspective for some engines and refrigerators*. Acoustical Society of America, Melville NY, 2002.

Gregory W. Swift, Scott N. Backhaus, and David L. Gardner. Us pat. no. 6032464, 2000.

K Tang, R Bao, G B. Chen, Y Qiu, L Shou, Z J. Huang, and T Jin. Thermoacoustically driven pulse tube cooler below 60 K. *Cryogenics*, 47:526–529, 2007.

M E. H. Tijani, J C. H. Zeegers, and A T. A. M. de Waele. Design of thermoacoustic refrigerators. *Cryogenics*, 42:49–57, 2002.

Y Ueda, T Biwa, U Mizutani, and T Yazaki. Experimental studies of a thermoacoustic Stirling prime mover and its application to a cooler. *Journal of the Acoustical Society of America*, 72(3):1134–1141, 2003.

Srinivas Vanapalli, Michael Lewis, Zhihua Gan, and Ray Radebaugh. 120 Hz pulse tube cryocooler for fast cooldown to 50 K. *Applied Physics Letter*, 90, 2007.

Martin Wetzel. *Experimental Investigation of a Single Plate Thermoacoustic Refrigerators.* PhD thesis, Johns Hopkins University, 1998.

J H. Xiao. Thermoacoustic heat transportation and energy transformation, part 3: Adiabatic wall thermoacoustic effects. *Cryogenics*, 35(1):27–29, 1995.

F. Zink, H. Waterer, R. Archer, and L. Schaefer. Geometric optimization of a thermoacoustic regenerator. *International Journal of Thermal Sciences*, 48:2309–2322, 2009.

Luke Zoontjens, Carl Q. Howard, Anthony C. Zander, and Ben S. Cazzolato. Modelling and optimisation of acoustic inertance segments for thermoacoustic devices. In *Proceedings of ACOUSTICS 2006*, pages 435–441, 2006.

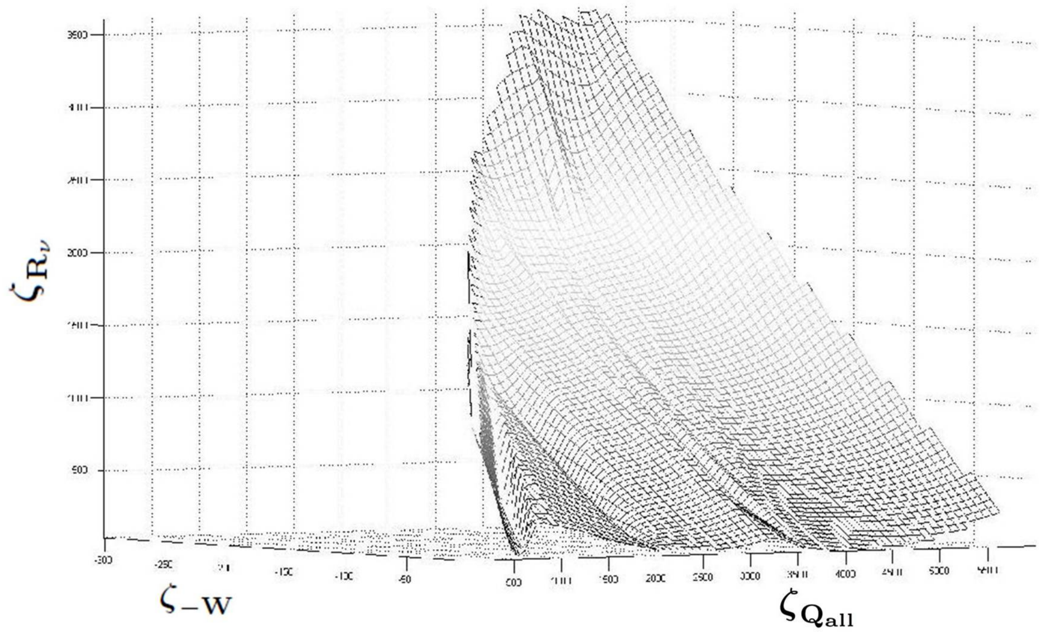

(a) Side profile of efficient frontier: simultaneously minimizing $-W$, R_ν, and Q_{all}

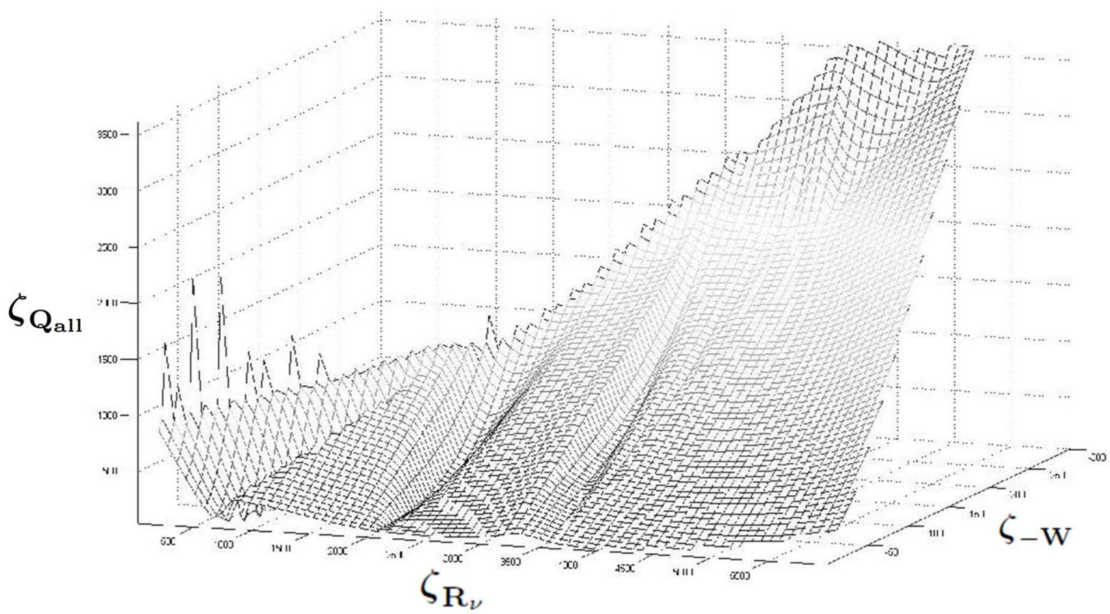

(b) Top profile of efficient frontier: simultaneously minimizing $-W$, R_ν, and Q_{all}

Figure 6: Two profiles from simultaneous minimization of $-W$, R_ν, and Q_{all}